Indian Journal of Pure & Applied Physics
Vol. 57, December 2019, pp. 891-899

Cubic methylammonium lead chloride perovskite as a transparent conductor in solar cell applications: An experimental and theoretical study

Paramita Sarkar, Rishikanta Mayengbam, S K Tripathy* & K L Baishnab

Department of Electronics and Communication Engineering,
National Institute of Technology, Silchar 788 010, India

Received 8 September 2018; accepted 29 August 2019

The cubic methylammonium lead chloride ($CH_3NH_3PbCl_3$) perovskite has been investigated as a transparent conductor using the experimental method and well-known density functional theory (DFT). The X-ray diffraction (XRD) of the as-prepared film confirms the good crystallinity and cubic phase of the material. The lattice constants are calculated from XRD data and compared with the lattice constants predicted employing DFT. The bandgap of the film has been studied to investigate the electronic properties and compared with the calculated bandgap of bulk $CH_3NH_3PbCl_3$ using DFT. In both the cases, the bandgap has been found to be direct in nature. Also, the partial and total density of states (PDOS and TDOS) have been discussed in detail. Further, the effective mass of electrons and holes are analyzed along the high symmetry points in the brillouin zone. The UV-VIS-NIR spectrometer has been used to measure the transmittance and reflectance of $CH_3NH_3PbCl_3$ film and established that films are highly transparent in visible and near IR regions. The optical properties such as dielectric functions, refractive index and absorption coefficients of bulk $CH_3NH_3PbCl_3$ perovskite have been calculated in the energy range 0-5 eV. All the calculated parameters are compared with the available experimental, and the theoretical state of art results and a fair agreement has been obtained between them.

Keywords: Perovskite, Transparent conductor, Optical properties, DFT, Experimental techniques

1 Introduction

In the recent past, perovskites with general formula ABX_3 where A and B are cations and X is anion have already gained significant attention due to their interesting structural, electronic, optical and magnetic properties. Among these perovskite materials, organo-lead halide perovskite materials with chemical formula $MAPbX_3$ (MA: $CH_3NH_3^+$, X= Cl^-, Br^- and I^-) have played a vital role in the field of solar cells, LEDs, photodetectors, lasers, thin film transistors and nonlinear optics[1]. These perovskite materials exhibit high carrier mobility, better carrier diffusion length, long charge carrier lifetime, and outstanding power conversion efficiency[2]. Recently, several attempts have been made to understand the structural, electronic and optical properties of pure and mixed halide perovskite materials for various applications[3-24]. The tolerance factor and phase transition under a temperature of methylammonium lead halide perovskites ($CH_3NH_3PbX_3$; X=Cl^-, Br^- and I^-) have been studied using solid-state principle[3,4] and IR spectroscopic studies[5], respectively. Further, single crystals and thin films of $CH_3NH_3PbX_3$ (X=Cl^-, Br^- and I^-) are prepared through different experimental techniques such as facile solution[6], hybrid sequential deposition process[7,8] and especially the low temperature, easy and cost-effective spin coating method[9] for varieties of optoelectronic applications[10]. To improve the stability, Valenzuela *et al.*[11] have prepared the mixed metal-organic halide perovskite and studied the structural, optical and photoluminescence properties. The single step and two step spin coating methods have been employed to synthesize uniform and pinhole-free $CH_3NH_3PbCl_3$ layer and fabricate a simple visible-blind UV photodiode device[12,13].

Various experimental and theoretical calculations have been carried out to understand the effective improvement of structural, electronic and optical properties of hybrid perovskites either by substituting or doping other materials in the cation and anion site[14-19]. Leguy *et al.*[20] have calculated the optical constants of $CH_3NH_3PbX_3$ (X=Cl^-, Br^- and I^-) employing density functional theory which is in line with experimental data. Further, Mosconi *et al.*[21] have measured the absorption coefficient of methylammonium lead chloride perovskites ($CH_3NH_3PbCl_3$) and found to be 0.46 at a bandgap of

*Corresponding author (E-mail: susanta96@gmail.com)

3.46 eV for tetragonal structure. Historically, oxide perovskites with equivalent or more bandgap are often used as the transparent conductors: indium doped Cd_3TeO_6 (3.92 eV)[22], $CaTiO_3$ (3.46 eV) and $PbTiO_3$ (3.4eV)[22-24]. Moreover, due to less availability and the high price of indium doped ITO, research has been carried out to substitute ITO with other transparent conductors. Although, $CH_3NH_3PbCl_3$ has a wide bandgap, small absorption coefficient, and better chemical stability which is suitable for transparent conductor applications. However, literature survey shows that no studies have been carried out on organic-inorganic halide perovskites as a transparent conductor except one[25].

Therefore, it has been thought of interest to study various properties of methylammonium lead chloride perovskites as a transparent conductor, particularly for solar cells application. In this paper, an attempt has been made to synthesize the methylammonium lead chloride perovskite ($CH_3NH_3PbCl_3$) film onto glass substrate via a one-step spin coating method. The x-ray diffraction (XRD) measurements and UV-VIS-NIR spectroscopy analysis have been done to study the structural and optical properties of synthesized films. Furthermore, first principle calculations using generalized gradient approximation (GGA) have been used to support and complement the experimental results.

2 Experimental Details

2.1 Materials and methodology

Lead chloride ($PbCl_2$, 98 %, Sigma-Aldrich), methylamine (CH_3NH_2, 33 wt % in absolute ethanol, Sigma-Aldrich), N, N-dimethylformamide (C_3H_7NO, anhydrous, 99.8 %, Sigma-Aldrich), hydrochloric acid (HCl, ACS reagent, 37 % in water, Sigma-Aldrich), diethyl ether ($(C_2H_5)_2O$, 98 %, Fisher Scientific) and dimethyl sulfoxide (C_2H_6OS, 99 % , Fisher Scientific) purchased and were used as received condition without any further purification.

Methylammonium chloride (CH_3NH_3Cl) was synthesized by following Wang *et al.*[1] method with few modifications. Typically, 16.85 mL of methylamine (0.338 mol) and 10.8 mL hydrochloric acid (0.355 mol) was added in a round-bottomed flask at room temperature and stirred at 1200 rpm for an hour, yielding a clear solution. The rotary evaporator was used for solvent evaporation, resulting in a white-yellow precipitate. The synthesized white-yellow precipitate was washed several times using diethyl ether and kept in the hot air oven at 60 °C for 24 h to obtain a white powder.

The $CH_3NH_3PbCl_3$ precursor solution was formed in dimethylformamide (DMF)/dimethyl sulfoxide (DMSO) solvent mixture (1/1 by volume). More specifically, CH_3NH_3Cl (0.007 mol, 0.482 gm) and $PbCl_2$ (0.007 mol, 1.986 gm) in an equimolar ratio were dissolved in the DMF/DMSO solvent mixture. The solution was stirred for 8 h at 60 °C before the deposition of the films. Filtration of the solution was done using the 0.45 micron PTFE filter. The films were coated by one step spin coating on the top of glass substrates at 6000 rpm for the 60 s at room temperature. Before the coating of films, the substrates were soaked in a soap solution, rinsed with ionized water, acetone and ethanol and dried in a hot air oven. The as-deposited perovskite films were annealed at 70 °C for 5 min in a hot air oven and followed by the annealing on a hot plate at 60 °C for 5 min. The detailed experimental procedure is shown in Fig. 1. Finally, the films were stored in a vacuum desiccator.

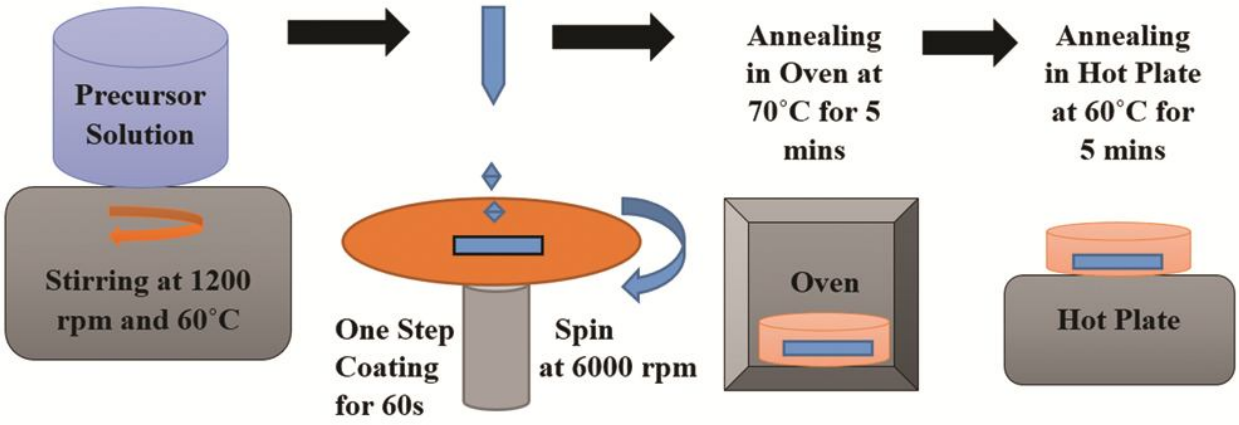

Fig. 1 — Experimental illustration of $CH_3NH_3PbCl_3$ perovskite film fabrication.

2.2 Theoretical method

The first principle calculations were done within the framework of density functional theory (DFT). The DFT calculations were executed using Atomistic Toolkit-Virtual Nanolab (ATK-VNL)[26] tool which works on a local combination of atomic orbitals (LCAO) methodology. The well-established generalized gradient approximation (GGA) with Perdew Burke Ernzerhof (PBE)[27, 28] was used to describe the exchange-correlation for the interaction of electrons. The density mess cut off was 250 Hartree (Ha), and self-consistent field (SCF) was set at 10^{-8} Ha throughout the calculation. The structural, optical and electronic properties were calculated using a dense k point sampling of 12×12×12 Monkhorst-Pack grid[29]. The limited memory Broyden Fletcher Goldfarb Shanno (LBFGS) optimization algorithm[30, 31] was used for the relaxation of ions. During this geometry optimization, the ions were permitted to relax until the force is less than 0.05 eV/Å.

3 Results and Discussion

3.1 Structural properties

The perovskite material with high purity and minimum defects are the key factors of solar cell applications. Therefore, specific attention has been paid to the synthesis procedure, more specifically in the selection of solvents. Maculan *et al.*[13] have synthesized $CH_3NH_3PbCl_3$ single crystal by an inverse temperature crystallization (ITC) method, and they have achieved best result using an equal-volume mixture of DMSO and DMF solvent at low temperature. By adopting this concept, in this work, the mixture of DMSO and DMF is used as the solvent for the precursor solution. The synthesis procedure of the $CH_3NH_3PbCl_3$ film has been illustrated in Fig. 1.

To study the crystal structure of the synthesized films, we have performed X-ray diffraction (XRD) measurement using Phillips X'Pert Pro Powder XRD (Cu K-alpha was1.5406 Å). The range of scanning angle, step size and step time were set to 10° to 60°, 0.02° and 0.50 s, respectively for the whole measurement. The XRD pattern of the $CH_3NH_3PbCl_3$ film is shown in Fig. 2, this established the purity as well as the crystallinity of the film. The reflection of the film has been further assured that the synthesized film is single phase $CH_3NH_3PbCl_3$ perovskite with preferential orientation along (100) direction. The pattern has shown no extra peaks of impurity phases except the cubic phase of $CH_3NH_3PbCl_3$ and the space group is Pm3m. The positions of the highest intensity and other prominent peaks are found at 15.49°, 31.36°, 35.20°, 47.90°; these observed 2θ peak positions are in good agreement with the reported cubic $CH_3NH_3PbCl_3$ crystals[6,14]. Here, the calculated lattice parameters are found to be a=b=c=5.710 Å which are very close to the other works[5-7,13]. In this work, we are looking for the possible application of $CH_3NH_3PbCl_3$ film as a transparent conductor for solar cell applications. Therefore, we have determined the average crystallite size (D)[11], lattice strain (ε)[32], dislocation density (δ)[33] and staking probability (α*)[10,34]. The calculated average crystallite size of the $CH_3NH_3PbCl_3$ film is found to be 115.72±3.88 nm. Our calculated crystallite size is in reasonably good agreement with earlier reported values[7,10,12] and also listed in Table 1. It is well known that an increase in crystallite size contributes to the decrease in crystal defects, lowers the trap state density and increases the electron lifetime[10,12].

Lattice strain can be defined as the strain which arises in lattice constants due to the crystal imperfections, and the lattice strain of 2.99×10^{-4} has been estimated from our observation. The lower value of strain leads to lower distortion of the crystal structure. The dislocation density (δ) is stated as the dislocation lines per unit area, and we have determined the density of 8.045×10^{13} lines/m^2, again

Table 1 — Lattice constants (Å), crystallite size (nm), bandgap (eV), transmittance (%) and static refractive index, and static dielectric constant of $CH_3NH_3PbCl_3$ perovskite (*experimental and #theoretical results).

Parameters	This work	Experimental results	Theoretical results using DFT
Lattice constants (Å) a=b=c	*5.710 #5.770	5.666[5], 5.6855[6], 5.65 [7], 5.67 [13]	5.840 [18], 5.750[18], 5.81[40]
Crystallite size (nm)	*115.72±3.88	55[7], 50[10], 50-200[12]	
Bandgap (eV)	*3.8 #2.6	3.1 [7, 15]	2.11[21], 2.34[40]
% Transmittance (%T)	*80<%T<97 in 300-1000 nm wavelength	80<%T<97[20] in 400-650 nm wavelength	
Static refractive index	#1.97		
Static dielectric constant	#3.9		4.8[19]

smaller values of δ is required for better crystallization of the film. The stacking fault probability of as-prepared film is 1.374×10^{-3}. The decreased value of dislocation density (δ), lattice strain (ε) and staking probability (α^*) can be attributed to the lesser imperfection in lattice and crystal defects. When these calculated values are compared with well-known transparent conductors used for the solar cells[35,36], these values are very convincing.

Further, the quantification of the strain of synthesized $CH_3NH_3PbCl_3$ film is possible by analyzing the line/peak broadening in the XRD pattern according to the Williamson and Hall technique (W-H). According to this, W-H technique, the average crystallite size and lattice strain contribute to the diffraction line/peak broadening. Based on the assumptions, Williamson and Hall have established a mathematical relation[37] as shown in Eq. (1):

$$\frac{\beta Cos\theta}{\lambda} = \frac{k}{D} + 2\varepsilon\left(\frac{2Sin\theta}{\lambda}\right) \quad \ldots(1)$$

Where 'k' is the shape factor, and its value is taken as 0.94, Cu K-alpha wavelength is represented by 'λ' and its value is 1.5406 Å, ε is the lattice strain, and D is average crystallite size. Also, 'θ' and 'β' are the Bragg's angle and full width at half maximum (FWHM), respectively. The values of 'θ' and 'β' are obtained from XRD data. We have plotted a graph between $\left(\frac{\beta cos\theta}{\lambda}\right)$ and $\left(\frac{2sin\theta}{\lambda}\right)$ in Fig. 3, which gives information about line broadening. Figure 3 shows that $\frac{\beta cos\theta}{\lambda}$ is a monotonous function of $\frac{2sin\theta}{\lambda}$ in all directions and discloses that line broadening is isotropic. The reciprocal of intercept drawn on the x-axis in the W-H plot gives the average crystallite size, and the slope provides the residual strain of the material. The crystallite size and strain are calculated using this method are found to be 121.40 nm and 2.45×10^{-4}, respectively. These obtained values of crystallite size (D) and lattice strain (ε) determined by W-H plot method are close to the values observed by Debye Scherrer's equation. The decreasing nature of the plot shows the compressive strain formed in the film. From the structural property analysis point of view, it is found that the films are well crystalline with minimum defect level, which are the key requirements for the film to act as transparent conducting material. When the results are compared with other commercially available transparent conducting materials, they are reasonably promising.

Moreover, structural analysis has been carried out using generalized gradient approximation (GGA) within the DFT framework. The organic-lead halide perovskite ($CH_3NH_3PbCl_3$) crystallizes in cubic phase at room temperature contains 12 atoms per unit cell with space group Pm3m and shown in Fig. 4.

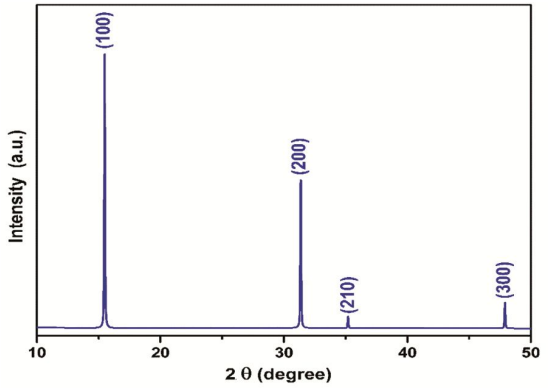

Fig. 2 — XRD spectra of $CH_3NH_3PbCl_3$ perovskite film.

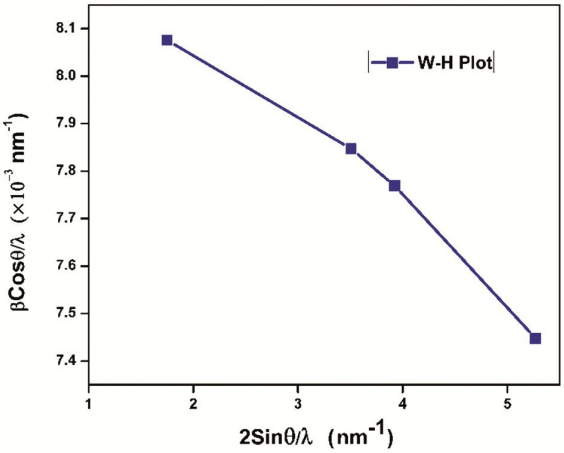

Fig. 3 — Williamson-hall plot for line broadening of $CH_3NH_3PbCl_3$ perovskite film.

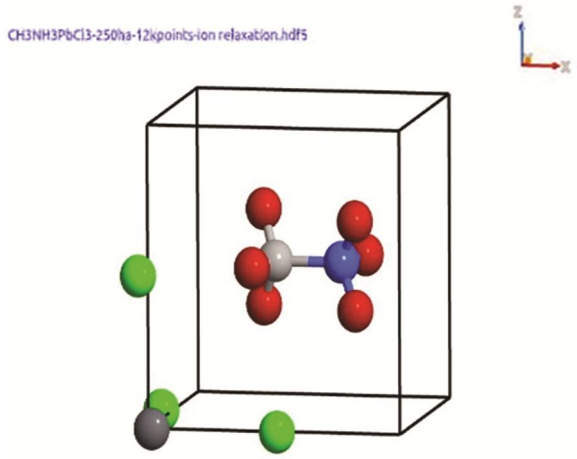

Fig. 4 — The unit cell geometry of bulk $CH_3NH_3PbCl_3$ perovskite. Color code: red (H), light gray (C), blue (N), dark gray (Pb) and green (Cl).

Further, the organic-lead halide perovskite structure has been optimized using our experimental lattice constant values. Fig. 5 shows the optimized structures of $CH_3NH_3PbCl_3$ (Z=4) with C-N bond oriented along the (100) direction. We have also optimized the total energy vs. volume and plotted in Fig. 6. The values of lattice constants have been calculated at minimum total energy and found to be a=b=c=5.770 Å. The calculated values of lattice constant are compared with other experimental results and other reported values and listed in Table 1. It is important to note that, our obtained values of lattice constants using DFT and experimental method are in good agreement.

3.2 Electronic properties

To better understand the atomistic properties of organic-lead halide perovskite it is important to study the electronic properties of the material. Bandgap determination is very important to exploit the possibility of $CH_3NH_3PbCl_3$ film as a transparent conductor in solar cells. In this work, Tauc's plot[38] is used to determine the experimental bandgap of synthesized films and given by Eq. (2):

$$(\alpha h\nu)^{1/n} = A\left(h\nu - E_g\right) \quad \ldots (2)$$

Where 'α' is called absorption coefficient, the value of 'A' is energy independent, 'ν' is the frequency, and band-gap and Planck's constant are denoted by 'E_g' and 'h', respectively. The values of 'n' are $^1/_2$, 2, 3, and $^3/_2$ for direct, indirect, forbidden indirect, and forbidden direct transition, respectively. The graph is plotted between $(\alpha h\nu)^2$ vs $(h\nu)$ to calculate the bandgap of the synthesized film[15] and shown in Fig. 7. It is found that the obtained direct bandgap for the film is 3.8 eV. Our synthesized cubic $CH_3NH_3PbCl_3$ films show 0.7 eV higher than the bandgap obtained previously[12,15]. However, the bandgap is depending on several parameters such as the experimental procedure, the thickness of films, crystallite size, defects, etc. So, this may be one of the reasons to have a higher bandgap compared to earlier researchers[12,15]. Also, the relatively higher bandgap achieved might be due to the less thickness of the films. Due to this wide bandgap, films show high transparency and fulfill the requirement of the transparent conductor. Historically, different types of perovskite oxides have been used as transparent conducting oxides (TCOs) and have also shown wide bandgap. Among those notable works, Tetsuka *et al*[22]. reported indium-doped Cd_3TeO_6 films coated on a glass substrate at high temperature by using magnetron

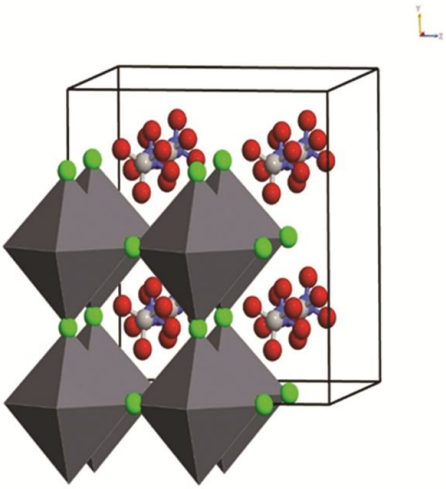

Fig. 5 — Relaxed cubo-octahedral structure of bulk $CH_3NH_3PbCl_3$ perovskite.

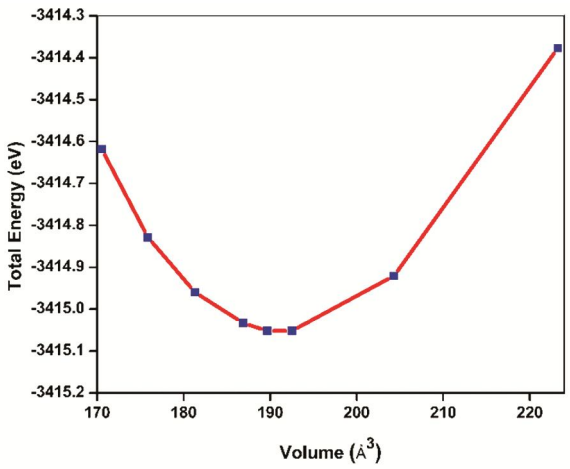

Fig. 6 — Total energy (eV) vs volume (Å^3) of bulk $CH_3NH_3PbCl_3$ perovskite.

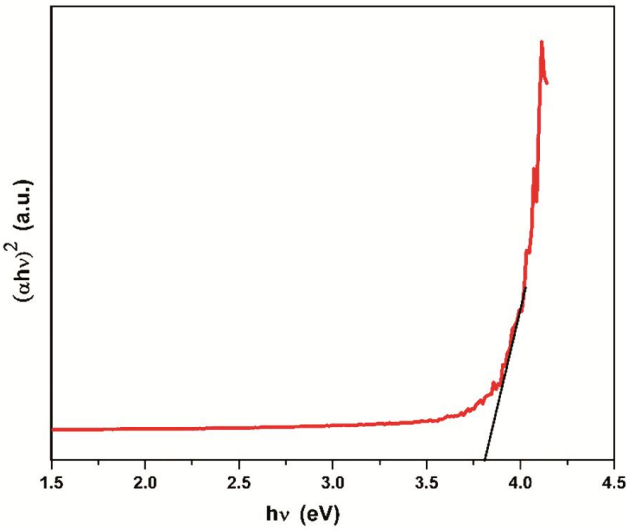

Fig. 7 — Tauc's plot for bandgap of $CH_3NH_3PbCl_3$ perovskite film.

sputtering method had shown direct band-gap of 3.9 eV which is almost equal to the bandgap acquired in this experiment. The obtained band-gap (3.8 eV) in this experiment is also in fair agreement with the bandgap of $CaTiO_3$ (~3.46 eV)[23] and $PbTiO_3$ (~3.4eV)[24] semiconductors, which are already investigated as a potential transparent conductor.

Moreover, using the optimized bulk structure of $CH_3NH_3PbCl_3$, the energy band of the material has been studied. In Fig. 8, the calculated energy band has been demonstrated in the energy range from -10 eV to +10 eV. The bandgap of $CH_3NH_3PbCl_3$ at R point is found to be 2.61 eV and direct in nature. Furthermore, it is generally known that GGA method mostly underestimates the bandgap[39]. Also, in our DFT calculation, we have used the bulk $CH_3NH_3PbCl_3$ material. It may be the reason due to which our obtained values of bandgap using experimental method is different for the DFT calculation. However, the calculated value of bandgap employing DFT has shown fair agreement with the theoretical value[21,40] and listed in Table 1. Moreover, the conduction band minimum has been found at 1.37 eV, and valence band maximum has been found at -1.21 eV. It confirms the p-type nature of $CH_3NH_3PbCl_3$ as predicted by earlier calculation[21]. Further, the electronic properties of the material analyzed in detail with the help of total density of states (TDOS) and partial density of states (PDOS). The density of states (DOS) calculation helps to understand the quantum chemistry of the compound. In Fig. 9, the PDOS and TDOS for C- s/p, H-s, N-s/p, Cl-s/p and Pb-s/p of $CH_3NH_3PbCl_3$ are shown. The Fermi level is set to zero. The valence band region from -10 eV to Fermi level (E_F) is subdivided into four regions. The leftmost region in the valence band, i.e., from -8.64 eV to -8.37 eV is contributed by N-p, Pb-s, and H-s with little contribution of C-p orbitals. The second region in the valence band, i.e. from -6.7 eV to -6.5 eV occurs due to the major contribution of N-p, C-p and minor contribution of Pb-s, and H-s states. The third region in the valence band is identified from -4.7 eV to -4.5 eV and mainly contributed by C-p, Pb-s, H-s, and admixture of N-p, Cl-p states. The rightmost region in the valence band from -3.57 eV to -0.30 eV is dominated by Cl-p orbital. In the conduction band region from 5.04 to 10 eV is mostly contributed by Pb-s and H-s states. Further, materials with direct bandgap >3 eV, lower effective mass and high transparency are highly desirable for transparent conductors. Therefore, for in-depth understanding, we have calculated the effective mass of electrons and holes of $CH_3NH_3PbCl_3$ material. It is well known that for n-type transparent conductors the effective mass of electrons should be lesser than the effective mass of holes. Whereas, for the p-type transparent conductor the effective mass of holes is lower compared to electrons[41]. In this work, the Fermi level is closer to a valence band which justifies that the material is of p-type. The effective masses of electrons (m_e) and holes (m_h) for cubic $CH_3NH_3PbCl_3$ have been calculated along with average effective mass using parabolic fitting of the band in each of the three symmetry directions around the R point of Brillouin zone and listed in Table 2. Here, the holes effective

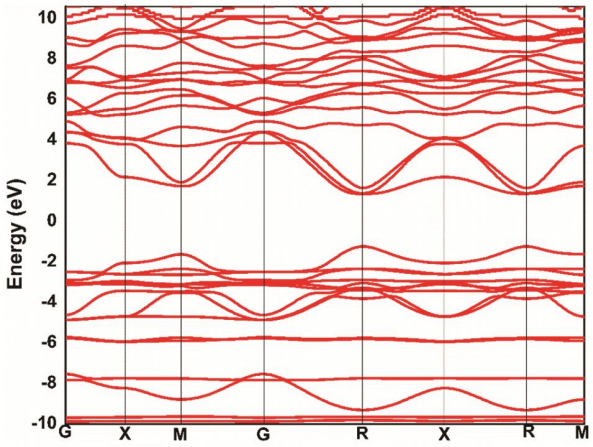

Fig. 8 — Calculated band-structure of bulk $CH_3NH_3PbCl_3$ perovskite.

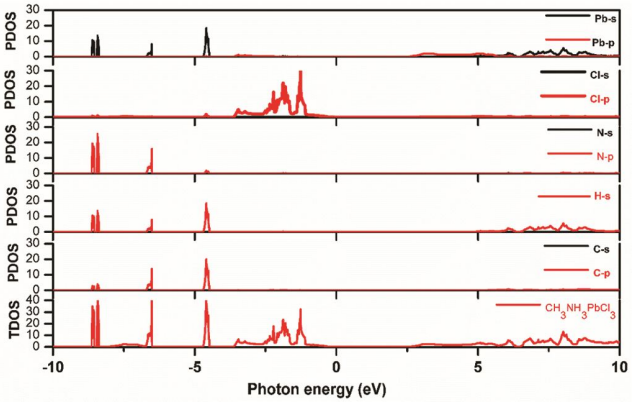

Fig. 9 — The PDOS and TDOS of bulk $CH_3NH_3PbCl_3$ perovskite.

Table 2 — Calculated effective masses along the symmetry directions R→X, R→M, R→G and their average for $CH_3NH_3PbCl_3$ perovskite.

$CH_3NH_3PbCl_3$	This work		Other reported values	
	m_e	m_h	m_e	m_h
R→X	1.12	0.26		
R→M	1.18	0.38		
R→G	1.49	0.39		
Average	1.26	0.34	0.54[39]	0.49[39]

mass is smaller compared to electrons. The top of the valence band dispersion comprises of the main contribution from the Cl-p orbital leading to a lower position of valence band maximum (VBM) which is very clear from Fig. 9. Whereas, the conduction band minimum (CBM) is mainly contributed by Pb-p state. Cl-p state is stronger in VBM compared to the Pb-p state in CBM. The strong Cl-p state is more delocalized than Pb-p and may be the reason behind a smaller effective mass of holes compared to electrons. Also, the calculated average effective masses in this work are compared with the results obtained by Welch *et al.*[42]. Our calculated average effective mass of electrons and holes are lager compared to Welch *et al.*[42]. The large average effective mass of both electrons and holes may be due to the different method adopted for DFT calculations.

3.3 Optical properties

The study of optical properties such as absorption coefficient, dielectric constant, refractive index, transmittance, and reflectance is utmost important for the materials to be used as a transparent conductor (TC). The UV-VIS-NIR spectrometer from Agilent technologies is used to identify the optical properties of the film in the wavelength range from 300-1000 nm. In this paper, we have characterized the film and found the percentage of transmittance 80 %-97 % in the wavelength range 300-1000 nm. Throughout the visible range (390-700 nm) as well as a portion of the near-infrared range (750-1000 nm) of light, films are highly transparent (97 %) and less reflective (~1.7 %) and shown in Fig. 10. To act as a base material for the transparent conductor, the high transparency of the film is one of the primary requirements of optical properties. The achieved transmittance (%) for this work is more than the reported work by Wang *et al.*[7] for $CH_3NH_3PbCl_3$ films synthesized by a sequential deposition process. Another noted work by Kumar *et al.*[25] has shown 90 % transmittance and less than 5 % of reflectance achieved for $CH_3NH_3BaI_3$ perovskite films on the glass substrate via a spin coating method.

In Fig. 11 the absorbance (a.u.) vs wavelength has been recorded after the baseline correction of the glass substrate for the $CH_3NH_3PbCl_3$ film. A good transparent conductor should not absorb light in the visible range. It is evident from Fig. 11 that the absorbance is about 0.013 (a.u.) which is minimal in the range of 390-1000 nm. The optical properties of $CH_3NH_3PbCl_3$ films conclude that the films are attaining high transmittance as well as the wide band-gap.

Moreover, the DFT calculated optical properties are demonstrated for $CH_3NH_3PbCl_3$ material. We have calculated the real $(\epsilon_1(\omega))$ and imaginary $(\epsilon_2(\omega))$ parts of the dielectric function, where $\epsilon_1(\omega)$ and $\epsilon_2(\omega)$ deal with the dispersion and absorption of incident light, respectively. The real part is deduced by using the Kramer-Kronig relationship, and the imaginary part is derived from the momentum matrix lie between unoccupied and occupied wave function. Further, using the relationship in Sun *et al.*[43], other optical properties such as absorption coefficient $\alpha(\omega)$ and refractive index $n(\omega)$ have been calculated. Figure 12 demonstrates the dielectric function of $CH_3NH_3PbCl_3$ in the energy range of 0-5 eV. From Fig. 12 it is seen that the calculated value of the static dielectric constant $\epsilon_1(0)$ is 3.9. It is already reported that the static dielectric constant follows a decreasing

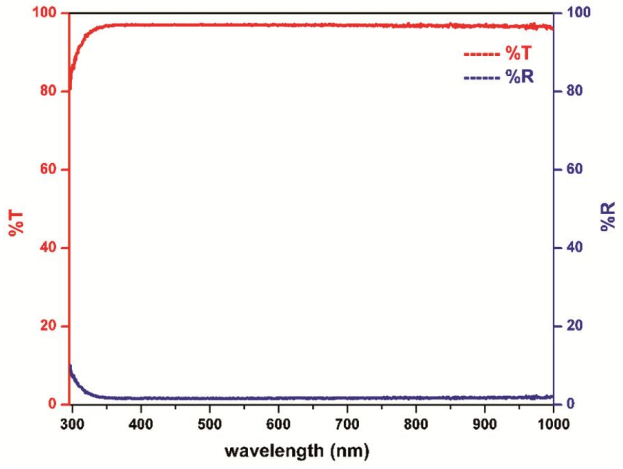

Fig. 10 — Transmittance (%T) and reflectance (%R) vs wavelength (nm) spectra of $CH_3NH_3PbCl_3$ perovskite film.

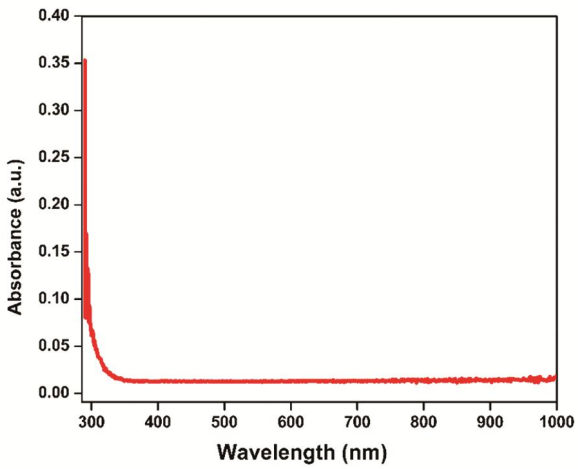

Fig. 11 — Absorbance (au) vs. wavelength (nm) spectra of $CH_3NH_3PbCl_3$ perovskite film.

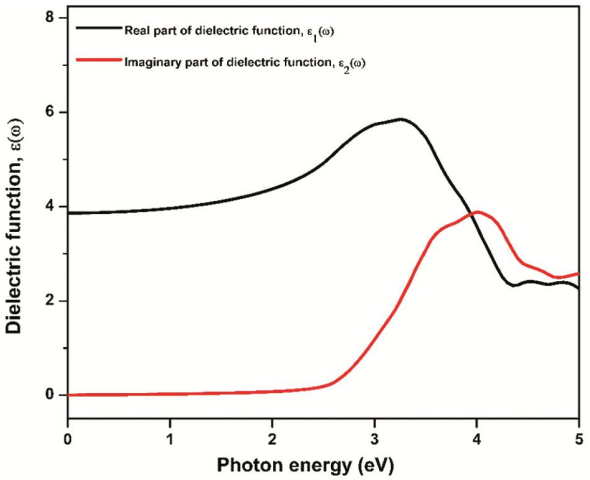

Fig. 12 — The calculated dielectric function of bulk $CH_3NH_3PbCl_3$ perovskite.

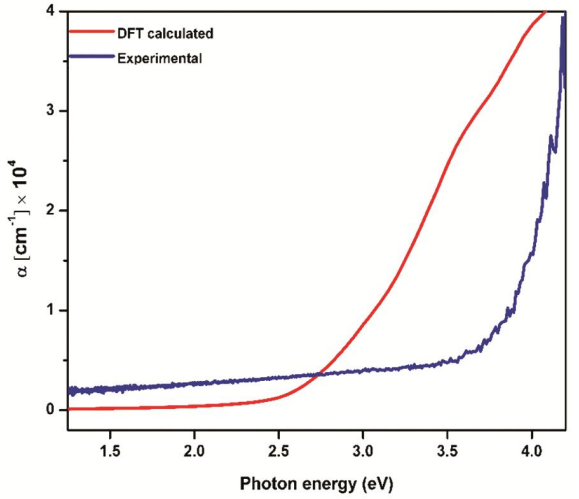

Fig. 13 — The absorption coefficient for bulk and film of $CH_3NH_3PbCl_3$ perovskite.

trend moving from I to Br, then to Cl in perovskite materials[19]. We have compared our calculated value of static dielectric constant with Filippetti *et al.*[19] and listed in Table 1.

The absorption coefficient $\alpha(\omega)$ of material defines the ability of light penetration into a material at a particular wavelength before the light gets absorbed. We have shown in Fig. 13 the calculated values of the absorption coefficient $\alpha(\omega)$ using experiment as well as DFT calculation in the energy range of 1-4 eV. The absorption coefficient has been observed at bandgap 2.61 eV (DFT calculated), and 3.8 eV (experimental) and the values of the absorption coefficient at band-gap is found to be 0.2×10^4 and 0.8×10^4 cm^{-1}, respectively. Unfortunately, there is no data available to compare the absorption coefficient of the cubic $CH_3NH_3PbCl_3$ material.

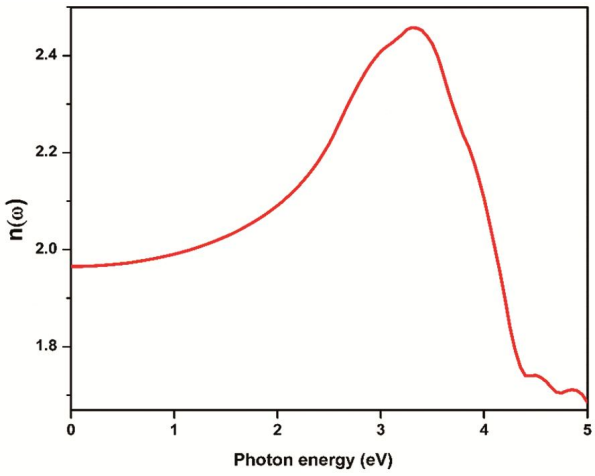

Fig. 14 — The refractive index of bulk $CH_3NH_3PbCl_3$ perovskite.

Figure 14 depicts the calculated refractive index of $CH_3NH_3PbCl_3$ in the energy range 0-5 eV. The calculated static refractive index is found to be 1.97 and presented in Table 1. We have compared the peaks obtained by Leguy *et al.*[20] and with our results. Also, it is found that at 3.3 eV the real part of dielectric constant start decreasing.

4 Conclusions

In conclusion, we have successfully synthesized highly transparent films of $CH_3NH_3PbCl_3$ perovskite onto glass substrates via a spin coating method. Almost 8 h solution processing in the ambient conditions was needed to achieve the well-crystalline and reproducible films. The structural and optical properties of the films have been investigated using an X-ray diffractometer and UV-VIS-NIR spectrometer, respectively. We have obtained a stable cubic perovskite structure with lattice constants a=b=c=5.710 Å and a band-gap of 3.8 eV. To complement the experimental results as well as to explore few other properties, DFT calculations were performed for bulk $CH_3NH_3PbCl_3$ perovskite material. The DFT calculated values of lattice constants, bandgap and absorption coefficient at bandgap are a=b=c=5.770 Å, 2.61 eV and 0.2×10^4 cm^{-1}, respectively. The calculated bandgap is less than the experimental bandgap which may be due to DFT calculations performed for bulk material. Further, the static dielectric constant and static refractive index have been reported as 3.9 and 1.97, respectively. Also, we have measured values of transmittance and absorbance as 97 % and 0.013 (a u), respectively in the visible region of light. Hence, this shows that the as-prepared film of $CH_3NH_3PbCl_3$ is highly

transparent in nature which may be a possible alternative for existing transparent conductors. All the above parameters were compared with the available experimental and theoretical values reported by other researchers.

Acknowledgment

This work is funded by Early Career Research scheme (File no. ECR/2016/001404) under SERB, New Delhi, Government of India. The authors are also thankful to CSIR, New Delhi for providing financial support. The authors are extending their gratitude to the SAIF, Department of Instrumentation & USIC, Guwahati University for XRD analysis. The authors are also thankful to Professor Sivaji Bandyopadhyay, Director, National Institute of Technology, Silchar for his continuous support in conducting this work.

References

1 Wang Q, Lyu M, Zhang M, Yun J, Chen H & Wang L, *J Phys Chem Lett*, 6 (2015) 4379.
2 Saparov B & Mitzi D B, *Chem Rev,* 116 (2016) 4558.
3 Travis W, Glover E N K, Bronstein H, Scanlon D O & Palgrave R G, *Chem Sci*, 7(2016) 4548.
4 Kieslich G, Sun S & Cheetham A K, *Chem Sci*, 5 (2014) 4712.
5 Mashiyama H & Kurihara Y, *J Korean Phys Soc*, 32(1998) S156.
6 Liu Y, Yang Z, Cui D, Ren X, Sun J, Liu X, Zhang J, Wei Q, Fan H, Yu F, Zhang X, Zhao C & Liu SF, *Adv Mater*, 27 (2015) 5176.
7 Wang W, Xu H, Cai J, Zhu J, Ni C, Hong F, Fang Z, Xu F, Cui S, Xu R, Wang L Xu F & Huang J, *Optics Express*, 24 (8) (2016) 8411.
8 Li N, Shi C, Li L, Zhang Z & Ma C, *Superlattices Microstruct*, 104 (2017) 445.
9 Kojima A, Teshima K, Shirai Y & Miyasaka T, *J Am Chem Soc*, 131 (2009) 6050.
10 Adinolfi V, Ouellette O, Saidaminov M I, Walters G, Abdelhady A L, Bakr O M & Sargent E H, *Adv Mater,* 28 (2016) 7264.
11 Montes-Valenzuela I, Pérez-Sánchez F & Morales-Acevedo A, *J Mater Sci: Mater Electron*, 29 (2018) 15404.
12 Zheng E, Yuh B, Tosado G A & Yu Q, *J Mater Chem C*, 5 (2017) 3796.
13 Maculan G, Sheikh A D, Abdelhady A L, Saidaminov M I, Haque M A, Murali B, Alarousu E, Mohammed O F, Wu T & Bakr O M, *J Phys Chem Lett*, 6 (2015) 3781.
14 Li X, Guo Y & Luo B, *Crystals*, 8 (2018) 4.
15 Zhang Z, Ren L, Yan H, Guo S, Wang S, Wang M & Jin K, *J Phys Chem C*, 121 (2017) 17436.
16 Wang S, Zhang W, Ma D, Jiang Z, Fan Z, Ma Q & Xi Y, *Superlattices Microstruct*, 113 (2018) 1.
17 Chai L, Zhong M, Li X, Wu N & Zhou J, *Superlattices Microstruct*, 120 (2018) 279.
18 Li J & Rinke P, *Phys Rev B*, 94 (2016) 045201.
19 Filippetti A & Mattoni A, *Phys Rev B*, 89 (2014) 125203.
20 Leguy A M A, Azarhoosh P, Alonso M I, Campoy-Quiles M, Weber O J, Yao J, Bryant D, Weller M T, Nelson J, Walsh A, Schilfgaarde M V & Barnes P R, *Nanoscale*, 8 (2016) 6317.
21 Mosconi E, Umari P & Angelis F D, *Phys Chem Chem Phys*, 18 (2016) 27158.
22 Tetsuka H, Shan Y J, Tezuka K, Imoto H & Wasa K, *J Mater Res*, 20 (2005) 2256.
23 Balachandran U, Odekirk B & Eror N G, *J Solid State Chem*, 41(1982)185.
24 Piskunov S, Heifets E, Eglitis R I & Borstel G, *Comput Mater Sci*, 29 (2004) 165.
25 Kumar A & Balasubramaniam K R, *Phys Rev B*, 94 (2016) 180105.
26 Berdiyorov G R, *AIP Adv*, 6 (2016) 055105.
27 Blöchl P E, *Phys Rev B*, 50 (1994) 17953.
28 Perdew J P, Burke K & Ernzerhof M, *Phys Rev Lett*, 77 (1996) 3865.
29 Monkhorst H J & Pack J D, *Phys Rev B*, 13 (1976) 5188.
30 Fischer T H & Almlof J, *J Phys Chem*, 96 (1992) 9768.
31 Mayengbam R, Tripathy S K, Palai G & Dhar S S, *J Phys Chem Solids*, 119 (2018) 193
32 Chopra K L, *Thin film phenomena*, (McGraw–Hill: New-York), 1st Edn, 1969.
33 Williamson G B & Smallman R C, *Philos Mag*, 1(1956) 34.
34 Pankaove J I, *Optical processed in semiconductors*, (Prentice-Hall: New Jerssey), 1st Edn, 1971.
35 Kondalkar V V, Mali S S, Pawar N B, Mane R M, Choudhury S, Hong C K, Patil P S, Patil S R, Bhosale P N & Kim J H, *Electrochim Acta*, 143 (2014) 89.
36 Turgut G, Keskenler E F, Aydın S, Yilmaz M, Dogan S & Duzgun B, *Phys Scr*, 87 (2013) 035602.
37 Williamson G K & Hall W H, *Acta Metall*, 1 (1953) 22.
38 Wang T, Daiber B, Frost J M, Mann S A, Garnett E C, Walsh A & Ehrler B, *Energy Environ Sci*, 10 (2017) 509.
39 Onida G, Reining L & Rubio A, *Rev Mod Phys*, 74 (2002) 601.
40 Mosconi E, Amat A, Nazeeruddin Md K, Grätzel M & Angelis F D, *J Phys Chem C*, 117 (2013) 13902.
41 Hautier G, Miglio A, Ceder G, Rignanese G –M & Gonze X, *Nat Commun*, 4 (2013) 2292.
42 Welch E, Scolfaro L & Zakhidov A, *AIP Adv*, 6 (2016) 125037.
43 Sun J, Wang H T, He J & Tian Y, *Phys Rev B*, 71 (2005) 125132.